



LAWRENCE
LIVERMORE
NATIONAL
LABORATORY

Mitigation of plasma-wall interactions with low-Z powders in DIII-D high confinement plasmas

F. Effenberg, F. Scotti

November 28, 2023

Nuclear Fusion

Disclaimer

This document was prepared as an account of work sponsored by an agency of the United States government. Neither the United States government nor Lawrence Livermore National Security, LLC, nor any of their employees makes any warranty, expressed or implied, or assumes any legal liability or responsibility for the accuracy, completeness, or usefulness of any information, apparatus, product, or process disclosed, or represents that its use would not infringe privately owned rights. Reference herein to any specific commercial product, process, or service by trade name, trademark, manufacturer, or otherwise does not necessarily constitute or imply its endorsement, recommendation, or favoring by the United States government or Lawrence Livermore National Security, LLC. The views and opinions of authors expressed herein do not necessarily state or reflect those of the United States government or Lawrence Livermore National Security, LLC, and shall not be used for advertising or product endorsement purposes.

Mitigation of plasma-wall interactions with low-Z powders in DIII-D high confinement plasmas

F. Effenberg¹, A. Bortolon¹, L. Casali², R. Nazikian³, I. Bykov³, F. Scotti⁴, H.Q. Wang³, M.E. Fenstermacher⁴, R. Lunsford¹, A. Nagy¹, B.A. Grierson³, F. M. Laggner¹, R. Maingi¹, and the DIII-D Team

1 - Princeton Plasma Physics Laboratory, Princeton, NJ 08543, USA

2 - University of Tennessee, Knoxville, TN 37996, USA

3 - General Atomics, San Diego, CA 92186, USA

4 - Lawrence Livermore National Laboratory, Livermore, CA 94550, USA

E-mail: feffenbe@pppl.gov

December 2021

Abstract. Experiments with low-Z powder injection in DIII-D high confinement discharges demonstrated increased divertor dissipation and detachment while maintaining good core energy confinement. Lithium (Li), boron (B), and boron nitride (BN) powders were injected in H-mode plasmas ($I_p = 1$ MA, $B_t = 2$ T, $P_{NB} = 6$ MW, $\langle n_e \rangle = 3.6 - 5.0 \cdot 10^{19} \text{ m}^{-3}$) into the upper small-angle slot (SAS) divertor for 2-s intervals at constant rates of 3-204 mg/s.

The multi-species BN powders at a rate of 54 mg/s showed the most substantial increase in divertor neutral compression by more than an order of magnitude and lasting detachment with minor degradation of the stored magnetic energy W_{mhd} by 5%. Rates of 204 mg/s of boron nitride powder further reduce ELM-fluxes on the divertor but also cause a drop in confinement performance by 24% due to the onset of an $n = 2$ tearing mode.

The application of powders also showed a substantial improvement of wall conditions manifesting in reduced wall fueling source and intrinsic carbon and oxygen content in response to the cumulative injection of non-recycling materials.

The results suggest that low-Z powder injection, including mixed element compounds, is a promising new core-edge compatible technique that simultaneously enables divertor detachment and improves wall conditions during high confinement operation.

Keywords: divertor power exhaust, dust injection, wall conditioning, detachment, powder injection, impurity seeding, core-edge integration

1. Introduction

Present plasma-facing component (PFCs) materials cannot withstand continuous heat fluxes above 10 MW/m² predicted for the next step large-scale fusion reactors such as ITER [1] or a projected future US fusion pilot plant [2]. Currently, tungsten is the high Z material choice for the ITER divertor, and recent and future world-leading reactor experiments [3, 4].

Dissipation and spreading of heat fluxes by isotropic low-Z impurity line emission are promising techniques to prevent melting and damage and extend the lifetime of the exposed wall materials. But overheating of PFCs cannot be avoided in high-Z, all-metal devices due to the lack of intrinsic low-Z impurity radiation. Therefore, low-Z impurities are injected in gaseous form to enhance divertor radiation or create a radiative mantle surrounding the hot core plasma [5]. Impurity gas seeding has been developed and extensively investigated, e.g. at the tokamaks TEXTOR[6], JET[5], Alcator C-Mod[7], ASDEX Upgrade [8], DIII-D [9], EAST [10], the heliotron LHD [11], and more recently at the stellarator W7-X [12].

The radiative power losses by low-Z impurities reduce the temperature and sputtering in the divertor. Plasma recombination sets on at temperatures below 1 eV and creates a protective neutral gas cushion in front of the targets, protecting against incoming heat and particle fluxes. In such a regime, the plasma boundary is removed from the divertor targets, and erosion and sputtering processes are substantially suppressed. This state is called plasma detachment [13, 14].

The radiative mantle and divertor dissipation approach aim to prevent damage and wear of main plasma-facing components to enable safe long-pulse operation. The ideal solution must be core-edge compatible, i.e., power losses in the boundary and divertor plasma must not have a detrimental impact on the high-performance core plasma.

Nitrogen gas is widely used for divertor dissipation since it effectively cools the plasma boundary. However, nitrogen is of concern in a reactor environment due to the production of tritiated ammonia (NT₃), which contaminate the uranium beds of the ITER tritium plant [15, 16]. Neon is of interest because it is a non-reactive high-recycling noble gas well suited for radiative mantle power exhaust. The choice of gases is eventually determined by their radiation characteristics and may be limited by chemistry [17, 18].

Numerical studies have suggested that alternative impurities such as boron (B) deserve consideration for radiative dissipation as well [19, 20]. However, boron delivery in gaseous form requires toxic or explosive gases like diborane (B₂D₆) or strongly diluted compounds such as trimethyl borane (C₃D₉B).

Lithium is under strong consideration as a liquid metal wall candidate potentially allowing to spread and conduct heat efficiently and safely away [21, 22, 23]. It is also promising for effective power dissipation using a particular lithium vapor box divertor design [24, 25].

More recently, the injection of low-Z solid materials in powder, dust or small granule form was introduced as a novel technique for various real-time applications. First applications focused on disruption mitigation [26], real-time wall conditioning [27, 28, 29, 30], mitigation of edge localized modes (ELMs) [31, 32], and enhancement of confinement properties [33, 34] which have been demonstrated with boron, boron nitride (BN), and lithium powders at T-10, DIII-D, EAST, ASDEX Upgrade, KSTAR, LHD, and W7-X.

Real-time powder injection provides easier access to a more extensive range of impurity species used for dissipative power exhaust. It facilitates the use of boron and lithium and multi-species mixtures such as boron nitride. In addition, it generally delivers impurities in higher purity without the bonding to fuel and other unwanted contaminants, as in the case of molecular gases.

In the present paper, first-time experiments at the DIII-D tokamak are presented where enhancement of divertor radiation was achieved during H-mode by injecting lithium, boron, and boron nitride powders into the upper closed small angle slot divertor. The closed divertor geometry generally facilitates the dissipation of heat and particle fluxes due to inherently better neutral compression [35, 36, 37, 38, 39].

2. Setup of low-Z powder injection in DIII-D high confinement plasmas

2.1. The upper single null H-mode target plasma

The experiments discussed in the following were conducted in upper-single null ELMy H-mode in standard and reversed toroidal field (B_t) direction ($I_p = 1.0$ MA, $B_t = 2$ T, $P_{NB} = 6$ MW, $\beta_n = 2.0$, $f_{ELM} = 80$ Hz, $n_e = 3.6 - 5.0 \cdot 10^{19}$ m⁻³). The outer strike point (OSP) is positioned in the small-angle slot divertor. In this configuration, the ion grad-B ($B \times \nabla B$) drift direction points away from (into) the SAS divertor in case of standard (reversed) toroidal B_t direction. Figure 1(a) shows the magnetic equilibrium, the location of the OSP at the SAS target, the powder injection location (green arrow), and the vertical camera view (DiMES TV [40]). The SAS geometry, the array of Langmuir probes (LP), the position of pressure gauges (PG), and the injection location of the impurity powder dropper (IPD) are shown in figure 1(b) in more detail. More properties of the SAS divertor are reported in [36, 35, 41].

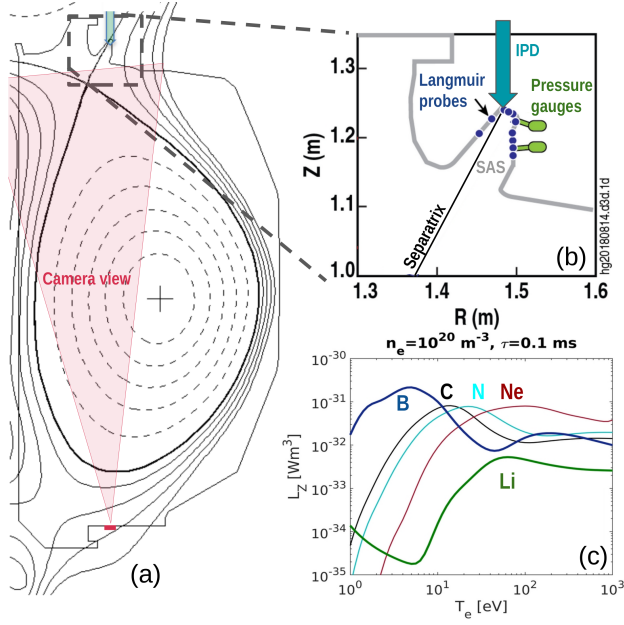


Figure 1. (a) Magnetic equilibrium and of upper single null H-mode scenarios. The arrow indicates the powder injection location in the small-angle slot divertor (SAS). (b) Langmuir probes and pressure gauges, impurity powder dropping location in the SAS divertor. (c) Cooling potentials L_Z for lithium, boron, carbon, nitrogen, and neon.

2.2. Low-Z impurity powder injection

The species-dependent cooling behavior of different elements used in radiative dissipation experiments is usually expressed by their radiation potential L_Z . It describes the cooling efficiency as a function of electron temperature. It is shown in figure 1(c) for boron, carbon, nitrogen, neon, and lithium, which entail the elements used in powder form in the present study (B, Li, BN) or conventional radiative power exhaust experiments (C, N, Ne). The total line emission has been calculated with atomic data from ADAS [42]. Boron shows for L_Z a maximum at 5 eV while lithium reaches its maximum at about 50 eV corresponding to far and near scrape-off layer (SOL) temperatures, respectively. Nitrogen shows peak radiation in between at 25 eV. The radiation potentials suggest that B, N, C causes power losses mainly in the SOL, while Li and Ne may radiate in the near SOL and around the separatrix. Yet, Li also has a secondary peak at one eV and causes additional radiative losses near the target of detached plasmas.

The impurity powder dropper (IPD) [43] is mounted at the top of the DIII-D tokamak device at a toroidal angle of 195°. The radial drop location is $R = 1.484$ m. It has four reservoirs filled with different types of impurity powders. Impurity powders were dropped directly into the OSP region through

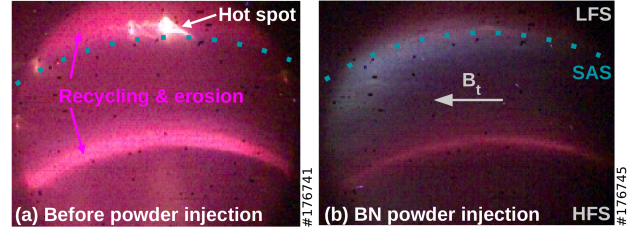


Figure 2. Vertical bottom-up view into closed divertor by visible camera (figure 1(a)) imaging (a) prior and (b) during boron nitride powder injection. The toroidal field direction (B_t), low field side (LFS), and high field side (HFS) are marked. The dashed line marks the position of the small angle slot (SAS) divertor. The bright emission belts and spots represent boundary emission from plasma-wall interactions and hot spot spots.

a tube of 2 m length into the SAS. The powder particles reach velocities of 5 – 6 m/s upon divertor entrance due to acceleration by gravitational force. The time delay between actuation and impact on the divertor plasma with the current DIII-D setup is typically 900 ms, whereas impurity gas feedback allows response within 100 ms. The divertor Langmuir probes and pressure gauge are used to characterize the divertor plasma. Additionally, vertical and tangential camera diagnostics measure visible and filtered line integrated brightness of different charge states of injected impurities [44, 40].

Impurities introduced in powder form do not immediately contribute to radiative losses. First, the macroscopic dust particles must undergo ablation, depending on the powder particle size and the sublimation energies. For example, lithium and boron nitride powders were of relatively fine size (40 and 65 μm), while the boron powder used consists of relatively large sizes (150 μm). Therefore, faster ablation is expected for lithium with sublimation energy of 19.59 J/mg while it is higher for boron with 46.98 J/mg.

3. Control of plasma-wall interactions with low-Z powder injection

3.1. Cooling of the plasma boundary with lithium and boron powders

In a sequence of experiments, boron, boron nitride, and lithium were injected in powder form in H-mode. The low-Z powders were released into the divertor plasma at 2.9 s. Mass flow rates of 3-204 mg/s were determined with a flow meter [43] corresponding to atomic rates of $0.2 - 5.4 \cdot 10^{21} \frac{\text{atoms}}{\text{s}}$.

A bottom-up camera view (figure 1(a)) was used to capture the visible emission from plasma-wall interactions on the high field side (HFS) and low field side (LFS) plasma-facing components. The emission is shown in figure 2(a) before and (b) during BN powder

injection of experiments conducted in the standard configuration with the ion grad-B drift pointing out of the upper SAS divertor. Before powder injection, bright emission was present at and near the outer and inner strike lines and the recycling regions (figure 2(a)). Also, a hot spot was detected on the low field side at a leading tile edge. The strong boundary emission at the low and high field sides results from neutral D_α and intrinsic impurities sputtered from the plasma-facing components. During injection of BN powder (≥ 200 mg/s), boundary emission and hot spot were suppressed (figure 2(b)).

During experiments with lithium and boron powder injections (3-35 mg/s), components of the spatial emission distributions are captured with the tangential camera. The camera filters extract Li II at 546 nm and B II at 410 nm, which are the only proxies for the spatial distribution of B and Li radiative power losses at this point. Since D_δ and C III emit within the band-pass of the filter used to image boron emission, background emission before boron injection was subtracted from the camera images. However, some residual contamination might remain due to a change of emissivity resulting from local cooling from the injected powder. The spatial brightness distributions are shown in figure 3 for single ionized lithium (a) and boron (b) at times during the injection, i.e., 5444 ms and 4258 ms, respectively. Vertical blue and green dashed lines in figure 3(a) and (b) indicate the innermost radial extent of the B II and Li II radiation zones. The Li II radiation is concentrated along the outer divertor leg, extending from the SAS volume to the X-point. The B II emission shows a different distribution. It shows stronger brightness in a layer close to the PFCs and extends in the radial direction outwards near the targets. There is almost no overlap in the spatial distributions between the Li II and B II radiation in the radial direction. The distinct features of the emission distribution of Li and B are consistent with the temperature dependency of the cooling potentials shown in figure 1(c). Boron cools the SOL while lithium causes temperature reduction in the vicinity of the separatrix. Unfortunately, during these first-time experiments, matching the powder flow rates between different species was not possible due to a lack of fine control. However, the results show substantial cooling of the divertor plasma with 3.3 mg/s lithium and 35 mg/s boron powder injection.

The time traces shown in figure 3(c-i) show a comparison of two representative H-mode plasmas with lithium and boron powder injections. The Li II and B II line emissivities begin to increase when the powder reaches the plasma after 3 seconds. The line averaged density remains almost stable, slightly increasing by 5% during lithium injection and dropping by 8% during

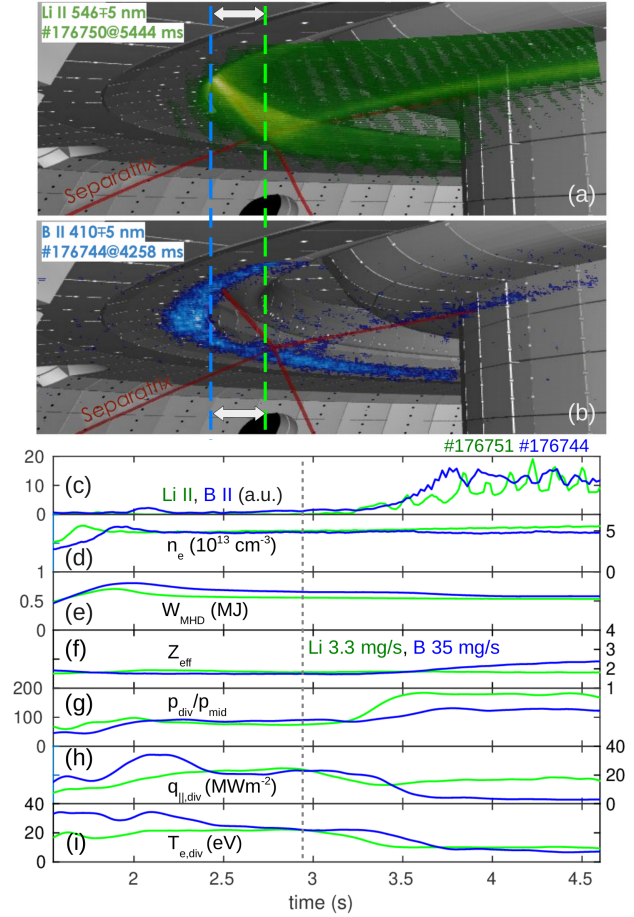


Figure 3. Line emissivities for (a) Li II (546 nm) and (b) B II (410 nm) were observed with tangential cameras. Vertical dashed lines indicate the innermost radial extent of the B II and Li II radiation zones. Time traces of (c) spectral line emissivities of Li II (546 nm) and B II (608 nm), (d) line averaged electron density, (e) stored magnetic energy W_{MHD} , (f) effective charge (Z_{eff}), (g) neutral compression (ratio of divertor-to-midplane pressure), (h) peak divertor parallel heat flux $q_{||,div}$, and (i) peak divertor electron temperature $T_{e,div}$. Lithium and boron powder injections start at ≈ 2.9 seconds.

boron injection. Z_{eff} remains constant in the case of Li but increases from 1.8 to 2.4 during B injection. The stored magnetic energy reduces by 5% in the case of Li. In the case of boron injection, a rate of 35 mg/s eventually triggers a $n = 2$ tearing mode which reduces stored magnetic energy by 14% after 3.5 s. Dilution effects are also estimated by measuring the rate of neutrons produced by deuterium-deuterium collisions during neutral beam injection. The measured neutron rates are related to the expected neutron emission based on a zero-dimensional calculation that includes the carbon density as the only impurity source [45] which allows estimating the dilution effects of injected impurities. The neutron rates prior to powder injection are $0.8 - 1.1 \times 10^{15}$ n/s, while it is estimated

that dilution of the plasma with lithium and boron impurities causes a reduction of maximum 10% and 25%. The neutral compression shown in figure 3(g) is defined as the ratio of divertor neutral pressure to main chamber pressure (measured at the outboard midplane). The divertor neutral gas pressure increases from 0.3 mtorr to 0.9 mtorr in the case of Li but only to 0.5 mtorr in the case of B injection. The divertor neutral compression increases by a factor of 3 and 1.5 following the lithium and boron powder injections. The peak electron temperatures and peak parallel heat fluxes measured with divertor Langmuir probes are shown in figure 3(h,i) reduce substantially after powder injection. In the case of low-rate Li powder injection, the peak electron temperature and heat flux are reduced by 12 eV and 10 MW/m^2 , respectively. A medium rate of B results in a reduction by 20 eV and heat flux detachment. At these relatively low rates, Li enhances the particle flux and density at the peak location contributing to a partial recovery of the parallel heat flux. On the other hand, the boron powder also reduces divertor particle flux and densities.

The results for B and Li powder injection show that core-edge compatibility may require some optimization of the divertor scenario in the future.

3.2. Sustained divertor detachment and strong neutral compression with boron nitride powder

More substantial injection with boron nitride at rates of 54 mg/s and above in configurations with ion $B \times \nabla B$ drift directed into the upper SAS divertor resulted in detachment and strong neutral compression. Figure 4(a-h) shows the time traces of line averaged density, stored magnetic energy, effective charge state Z_{eff} , divertor neutral compression, neutral deuterium emission in the divertor D_α and the divertor peak parallel heat fluxes and electron temperatures in the divertor. Divertor heat fluxes and temperature rapidly decrease and remain suppressed during BN injection. The increase in divertor neutral gas compression by more than one order of magnitude means a substantial contribution to dissipation by ion-neutral friction forces in the small-angle slot divertor. The D_α emission shows that ELM-fluxes in the divertor reduce in frequency for 54 mg/s and further reduce in amplitude at a very high rate of 204 mg/s due to dissipation. The effective charge Z_{eff} increases from base level by 0.8 to 2.3 while the stored magnetic energy W_{mhd} drops from 0.7 MJ by 5% during 54 mg/s BN injection. At the high rate of 204 mg/s , energy confinement drops by 24% due to an $n = 2$ tearing mode triggered after 3.8 s and Z_{eff} increases to 4.5. Using the approach mentioned above, the rate of neutrons reduces by up to 28%-38% at higher BN powder injection rates ($54\text{-}204 \text{ mg/s}$) due to dilution

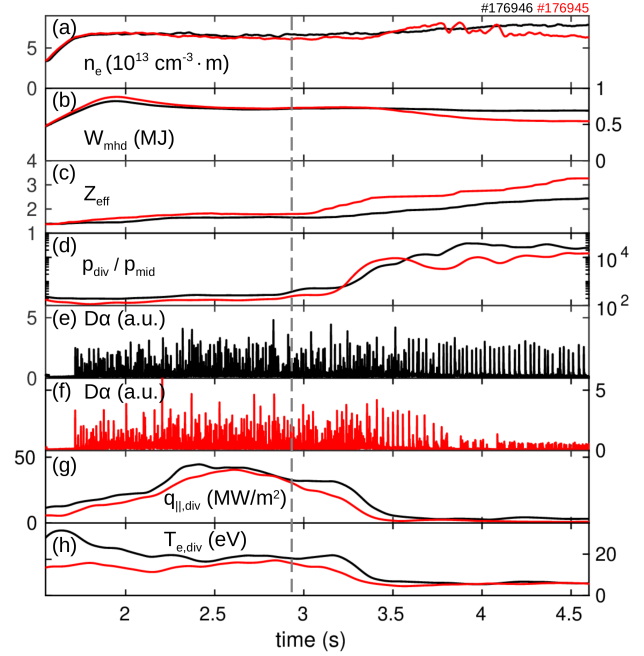


Figure 4. Time traces for boron nitride (BN) at high injection rates of 54 mg/s (black) and 204 mg/s (red). (a) line averaged electron density (b) stored magnetic energy W_{mhd} , (c) effective charge Z_{eff} , (d) divertor neutral compression, (e, f) divertor neutral emission D_α , (g) peak divertor parallel heat flux $q_{||,div}$, and (h) peak divertor electron temperature $T_{e,div}$. The powder injection starts at ≈ 2.9 seconds.

effects on the core plasma.

The rate of neutrons produced during deuterium-deuterium collisions during neutral beam injection has dropped to 62% of the initial level ($8.8 \cdot 10^{14} \text{ n/s}$) at 4.5 s due to dilution effects on the core plasma during moderate and high BN injection ($54\text{-}204 \text{ mg/s}$). However, the neutron rates (up to $1 \cdot 10^{15} \text{ n/s}$) were maintained without or with only more minor losses during other scenarios with low-Z powder injection. Therefore, it is suggested that the core-edge compatibility can be optimized by modifying the injection rates and powder mix for a specific plasma scenario.

3.3. Improving wall conditions

Successive powder injections into the upper divertor during these experiments resulted in a significant improvement of wall conditions similar to experiments in lower single null with injection into the plasma crown reported in [28]. The strongest effects of wall conditioning were measured during the first sequence of experiments with boron powder injection. In figure 5, the time traces of (a) D_α , (b) main chamber neutral pressure p_{mid} , (c) C IV and (d) O IV are shown for the initial L-mode phase ($< 1.6 \text{ s}$) for the first

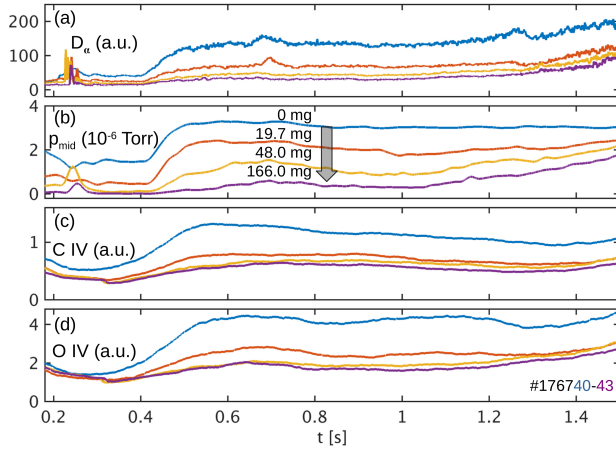


Figure 5. Change in wall conditioning before and after boron powder injection represented by time traces of (a) D_α line emission in the divertor, (b) main chamber neutral pressure p_{mid} measured at the midplane, (c) C IV (384 nm) emission, and (d) O IV (555 nm) emission during initial L-mode phase. The cumulative mass (mg) of boron powder deposited prior to each experiment is indicated.

sequence of experiments. The cumulative amounts of boron powder deposited during each of the previous discharges are indicated.

D_α and main chamber neutral pressure reduce after each discharge with boron powder injection. The reduction in D_α emission and neutral pressure suggests a decrease of the intrinsic neutral source, i.e., wall recycling and out-gassing. Higher levels of neutral gas are injected to achieve the same target density following B injections. At the same time, CIV and OIV brightness reduce, which suggests a reduction in the intrinsic impurity source. A reduction in the impurity line emission may in parts be due to an increase in the boundary plasma temperature following a reduction in density. Unfortunately, no upstream SOL electron temperature measurements are available in this case. The wall conditioning metric shown in figure 6 is defined as the ratio between deuterium gas input and line averaged electron density $\propto \frac{\Gamma_{D2}}{n_e}$ evaluated during the L-mode phase. Improving wall conditions based on this metric means reducing the intrinsic neutral source, which allows for better plasma density control through external gas input. A better density control through improved wall conditions was achieved, expressed in the ratio between gas input and density sharply increasing during the first boron injection experiments. Wall conditioning matures following BN powder injection and does not improve further following Li powder injection.

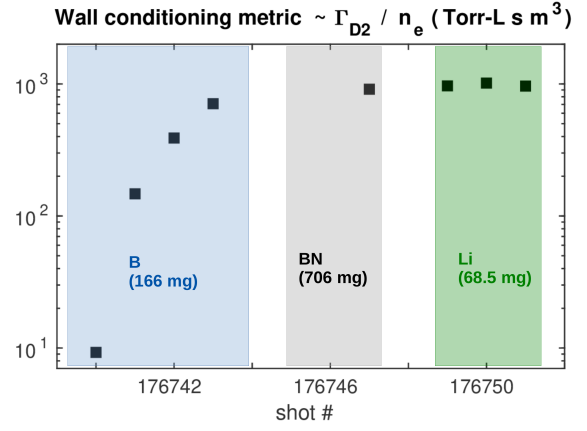


Figure 6. Shot-by-shot change of the ratio of deuterium gas input Γ_{D2} to electron density n_e (wall conditioning metric), which have been calculated as an average value over a 1.2 s time window (from $t = 0.3$ s to 1.5 s) during the initial L-mode phase. The cumulative amounts of powder are indicated in mg for each powder type.

4. Discussion

Low-Z powder injection has been very suitable for reducing heat fluxes, increasing neutral build-up in the divertor, and improving wall conditions by forming low recycling coatings on the main plasma-facing components. The application of different impurity powders revealed some essential effects. Boron was suitable for cooling divertor heat fluxes and temperatures and showed the most significant improvement in wall conditions. However, it showed less effectiveness regarding divertor neutral compression. Figure 7(a) shows the change in divertor neutral gas compression during single and multi-species powder injection. Boron shows even at increasing injection rate no further increase in neutral compression. In contrast, it shows a steady increase in change of Z_{eff} as shown in figure 7(b), and also a stronger dilution effect on the neutron source than lithium.

The neutral compression is higher and increases further with lithium and boron nitride injection. Moreover, the latter affect Z_{eff} much less than boron.

The data show that higher rates of powder injection, i.e., several tens in case of large-grained boron and several hundreds of mg/s in case of fine-grained BN increase the risk of the onset of tearing modes. These tearing modes are detrimental for confinement and also occur during radiative mantle and radiative divertor experiments with impurity gas seeding [46].

The analysis of wall conditioning suggests that B is more effective than BN and Li. This can be attributed to differences in powder particles sizes and ablation,

allowing the larger B particles to escape the divertor and condition larger wall surface areas than Li and BN.

Lithium powders injected only at low rates showed increased divertor density and particle fluxes. Future modeling will be used to further disentangle the effects of particle size, injection rates, radiation behavior, and potentially drift effects on the divertor plasma distribution.

The wall conditioning effects observed are generally consistent with results reported earlier for dedicated real-time wall conditioning experiments in lower single null configurations [27, 28]. An important difference in the present work is to have the injection location downstream in the divertor (compared to an injection location in the plasma crown in the previous studies). The experiments presented in this work show that wall conditions can also be improved by injecting large-sized boron powder into the divertor. The line emission distributions obtained with tangential cameras are consistent with the temperature dependencies of the cooling potentials shown in figure 1(c) for the respective impurities. The data suggest that boron radiates at lower scrape-off layer temperatures than lithium, which may help optimize the SOL-to-core fraction in radiative losses.

An advantage compared to gas injection is that materials can be delivered in pure form (no dilution through additional hydrogen bonding, as in the case of methane or diborane) and are not toxic or explosive. The injection technique of solid material is presently relatively slow due to mechanical friction and dependence on gravitational acceleration. However, recent studies at EAST and KSTAR have shown promising results regarding real-time wall conditioning in long pulse [47, 29]. Electromagnetic acceleration may also increase the real-time capabilities of solid material injection for applications requiring a shorter response time [48].

5. Conclusions

Divertor dissipation with single and multi-species low-Z powder injection has been demonstrated at DIII-D in a USN closed divertor (SAS) configuration during H-mode. The increase in divertor dissipation is expressed by a substantial reduction of divertor temperatures and heat fluxes, increased divertor neutral compression, and transition into detachment, which usually comes at the price of a slight decrease in confinement parameters by 5-10%. Lithium and boron nitride enhance the neutral compression at lower rates due to their smaller particle size. In contrast, larger boron dust particles show less neutral compression and higher core contamination than Li and BN. The onset of tearing modes was observed at 35 mg/s for boron. The

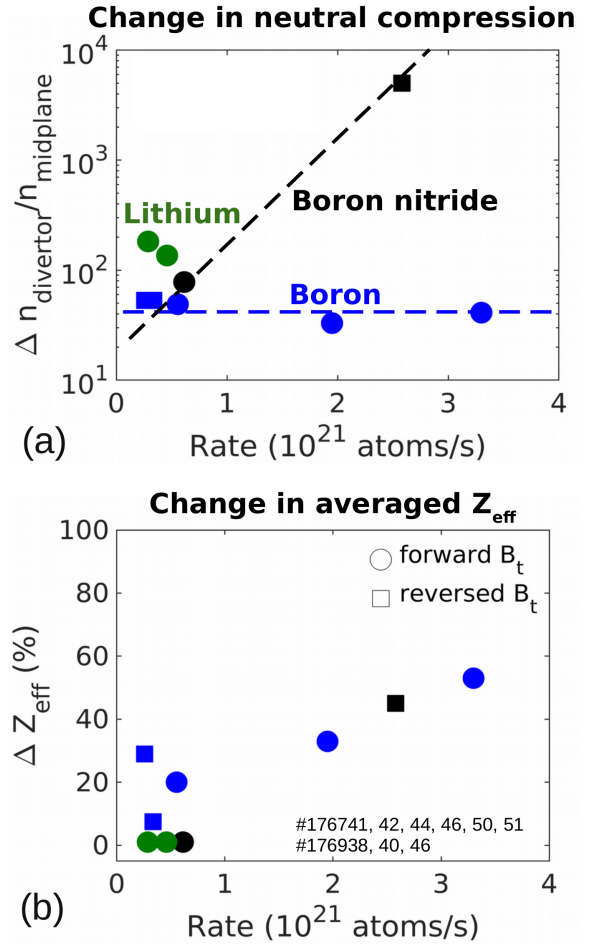


Figure 7. (a) Change in divertor neutral gas compression and (b) change in Z_{eff} for B, BN, Li in forward and reversed B_t .

most substantial level of detachment with only small confinement degradation was achieved with 54mg/s BN injection in a reversed B_t configuration (ion grad B drift pointing away from the X-point into the SAS). Very high rates of BN (204 mg/s) substantially reduce ELM fluxes but cause losses of 24% to W_{mhd} due to the onset of tearing modes. The observed trends suggest that optimizing the flow rates may allow a good balance between sufficient divertor dissipation and low confinement degradation. Wall conditions also improved significantly after injecting powders into the closed divertor showing a substantial reduction in recycling, carbon, and oxygen levels. Low-Z powder injection into the divertor is a promising new approach to suppress high heat fluxes to the divertor targets and improve core-edge compatibility.

Acknowledgements

This material is based upon work supported by the U.S. Department of Energy, Office of Science,

Office of Fusion Energy Sciences, using the DIII-D National Fusion Facility, a DOE Office of Science user facility, under Awards DE-AC02-09CH11466, DE-FC02-04ER54698, and DE-AC52-07NA27344. The DIII-D data shown in this paper can be obtained in digital format by following the links at https://fusion.gat.com/global/D3D_DMP. The United States Government retains a non-exclusive, paid-up, irrevocable, world-wide license to publish or reproduce the published form of this manuscript, or allow others to do so, for United States Government purposes. The author Florian Effenberg gratefully acknowledges discussions with Galen Burke, Houyang Y. Guo, Adam McLean, Charles J. Lasnier, Jun Ren, Morgan W. Shafer, and Dinh Truong.

Disclaimer

This report was prepared as an account of work sponsored by an agency of the United States Government. Neither the United States Government nor any agency thereof, nor any of their employees, makes any warranty, express or implied, or assumes any legal liability or responsibility for the accuracy, completeness, or usefulness of any information, apparatus, product, or process disclosed, or represents that its use would not infringe privately owned rights. Reference herein to any specific commercial product, process, or service by trade name, trademark, manufacturer, or otherwise does not necessarily constitute or imply its endorsement, recommendation, or favoring by the United States Government or any agency thereof. The views and opinions of authors expressed herein do not necessarily state or reflect those of the United States Government or any agency thereof.

References

- [1] R. A. Pitts, S. Carpentier, F. Escourbiac, T. Hirai, V. Komarov, S. Lisgo, A. S. Kukushkin, A. Loarte, M. Merola, A. S. Naik, R. Mitteau, M. Sugihara, B. Bazylev, P. C. Stangeby, A full tungsten divertor for ITER: Physics issues and design status, *Journal of Nuclear Materials* 438 (2013) S48 – S56. doi:10.1016/j.jnucmat.2013.01.008.
- [2] National Academy of Engineering, E. National Academies of Sciences, and Medicine, Bringing Fusion to the U.S. Grid, The National Academies Press, Washington, DC, 2021. doi:10.17226/25991.
- [3] C. Linsmeier, M. Rieth, J. Aktaa, T. Chikada, A. Hoffmann, J. Hoffmann, A. Houben, H. Kurishita, X. Jin, M. Li, A. Litnovsky, S. Matsuo, A. v. Müller, V. Nikolic, T. Palacios, R. Pippan, D. Qu, J. Reiser, J. Riesch, T. Shikama, R. Stieglitz, T. Weber, S. Wurster, J.-H. You, Z. Zhou, Development of advanced high heat flux and plasma-facing materials, *Nuclear Fusion* 57 (9) (2017) 092007.
- [4] J. W. Coenen, S. Antusch, M. Aumann, W. Biel, J. Du, J. Engels, S. Heuer, A. Houben, T. Hoeschen, B. Jasper, F. Koch, J. Linke, A. Litnovsky, Y. Mao, R. Neu, G. Pintsuk, J. Riesch, M. Rasinski, J. Reiser, M. Rieth, A. Terra, B. Unterberg, Th. Weber, T. Wegener, J.-H. You, C. Linsmeier, Materials for DEMO and reactor applications—boundary conditions and new concepts, *Physica Scripta* 2016 (T167) (2016) 014002.
- [5] G. P. Maddison, C. Giroud, G. K. McCormick, J. A. Alonso, B. Alper, G. Arnoux, P. C. d. S. A. Belo, M. N. A. Beurskens, A. Boboc, S. Brezinsek, I. Coffey, S. Devaux, T. Eich, W. Fundamenski, D. Harting, A. Huber, S. Jachmich, I. Jenkins, E. Joffrin, M. A. H. Kempenaars, M. Lehnen, T. Loarer, P. J. Lomas, A.G. Meigs, P. D. Morgan, V. Riccardo, F. G. Rimini, M. F. Stamp, G. Telesca, H. Thomsen, J. E. contributors, Moderation of divertor heat loads by fuelling and impurity seeding in well-confined ELMy H-mode plasmas on JET, *Nuclear Fusion* 51 (4) (2011) 042001.
- [6] U. Samm, G. Bertschinger, P. Bogen, J. D. Hey, E. Hintz, L. Konen, Y. T. Lie, A. Pospieszczyk, D. Rusbuldt, R. P. Schorn, B. Schweer, M. Tokar, B. Unterberg, Radiative edges under control by impurity fluxes, *Plasma Physics and Controlled Fusion* 35 (SB) (1993) B167–B175, publisher: IOP Publishing. doi:10.1088/0741-3335/35/sb/013.
- [7] M. Reinke, J. Hughes, A. Loarte, D. Brunner, I. Hutchinson, B. LaBombard, J. Payne, J. Terry, Effect of n₂, ne and ar seeding on alcator c-mod h-mode confinement, *Journal of Nuclear Materials* 415 (1, Supplement) (2011) S340–S344, proceedings of the 19th International Conference on Plasma-Surface Interactions in Controlled Fusion. doi:https://doi.org/10.1016/j.jnucmat.2010.10.055.
- [8] A. Kallenbach, M. Bernert, M. Beurskens, L. Casali, M. Dunne, T. Eich, L. Giannone, A. Herrmann, M. Maraschek, S. Potzel, F. Reimold, V. Rohde, J. Schweinzer, E. Viezzer, M. Wischmeier, the ASDEX Upgrade Team, Partial detachment of high power discharges in ASDEX Upgrade, *Nucl. Fusion* 55 (5) (2015) 053026. doi:10.1088/0029-5515/55/5/053026.
- [9] L. Casali, T. H. Osborne, B. A. Grierson, A. G. McLean, E. T. Meier, J. Ren, M. W. Shafer, H. Wang, J. G. Watkins, Improved core-edge compatibility using impurity seeding in the small angle slot (SAS) divertor at DIII-D, *Physics of Plasmas* 27 (6) (2020) 062506. doi:10.1063/1.5144693.
- [10] J. Chen, Y. Duan, Z. Yang, L. Wang, K. Wu, K. Li, F. Ding, H. Mao, J. Xu, W. Gao, L. Zhang, J. Wu, G.-N. L. and, Radiative divertor behavior and physics in ar seeded plasma on EAST, *Chinese Physics B* 26 (9) (2017) 095205. doi:10.1088/1674-1056/26/9/095205. URL <https://doi.org/10.1088/1674-1056/26/9/095205>
- [11] T. Morisaki, K. Oyama, N. Tamura, S. Masuzaki, T. Akiyama, G. Motojima, J. Miyazawa, B. J. Peterson, N. Ohno, H. Yamada, Radiated power distributions in impurity-seeded plasmas in LHD, *Journal of Nuclear Materials* 463 (2015) 640 – 643. doi:http://dx.doi.org/10.1016/j.jnucmat.2015.01.016.
- [12] F. Effenberg, S. Brezinsek, Y. Feng, R. König, M. Krychowiak, M. Jakubowski, H. Niemann, V. Perseo, O. Schmitz, D. Zhang, T. Barbui, C. Biedermann, R. Burhenn, B. Buttenschön, G. Kocsis, A. Pavone, F. Reimold, T. Szepesi, H. Frerichs, Y. Gao, U. Hergenhan, S. Kwak, M. Otte, T. S. P. and, First demonstration of radiative power exhaust with impurity seeding in the island divertor at Wendelstein 7-X, *Nuclear Fusion* 59 (10) (2019) 106020, publisher: IOP Publishing. doi:10.1088/1741-4326/ab32c4.
- [13] G. F. Matthews, Plasma detachment from divertor targets and limiters, *Journal of Nuclear Materials* 220-222 (1995)

- 104 – 116. doi:10.1016/0022-3115(94)00450-1.
- [14] S. I. Krashennikov, A. S. Kukushkin, A. A. Pshenov, Divertor plasma detachment, *Physics of Plasmas* 23 (5) (2016) 055602. doi:10.1063/1.4948273.
- [15] D. Neuwirth, V. Rohde, T. S.-S. and, Formation of ammonia during nitrogen-seeded discharges at ASDEX upgrade, *Plasma Physics and Controlled Fusion* 54 (8) (2012) 085008. doi:10.1088/0741-3335/54/8/085008.
- [16] L. Laguardia, R. Caniello, A. Cremona, G. Gatto, G. Gervasini, F. Ghezzi, G. Granucci, V. Meller, D. Minelli, R. Negrotti, M. Pedroni, M. Realini, D. Ricci, N. Rispoli, A. Uccello, E. Vassallo, Influence of he and ar injection on ammonia production in n2/d2 plasma in the medium flux gym device, *Nuclear Materials and Energy* 12 (2017) 261–266, proceedings of the 22nd International Conference on Plasma Surface Interactions 2016, 22nd PSI. doi:https://doi.org/10.1016/j.nme.2017.05.009.
- [17] A. Kallenbach, M. Bernert, R. Dux, L. Casali, T. Eich, L. Giannone, A. Herrmann, R. McDermott, A. Mlynek, H. W. Müller, F. Reimold, J. Schweinzer, M. Sertoli, G. Tardini, W. Treutterer, E. Viezzer, R. Wenninger, M. W. and, Impurity seeding for tokamak power exhaust: from present devices via ITER to DEMO, *Plasma Physics and Controlled Fusion* 55 (12) (2013) 124041, publisher: IOP Publishing. doi:10.1088/0741-3335/55/12/124041.
- [18] R. J. Walker, M. R. Gilbert, Neutron activation of impurity seeding gases within a DEMO environment, *Fusion Engineering and Design* 124 (2017) 892 – 895. doi:10.1016/j.fusengdes.2017.01.057.
- [19] A. Y. Pigarov, Radiative detached divertor with acceptable separatrix Z_{eff} , *Physics of Plasmas* 24 (10) (2017) 102521. doi:10.1063/1.4986516.
- [20] F. Effenberg, A. Bortolon, H. Frerichs, B. Grierson, J. Lore, T. Abrams, T. Evans, Y. Feng, R. Lunsford, R. Maingi, A. Nagy, R. Nazikian, D. Orlov, J. Ren, D. Rudakov, W. Wampler, H. Wang, 3d modeling of boron transport in diii-d l-mode wall conditioning experiments, *Nuclear Materials and Energy* 26 (2021) 100900. doi:10.1016/j.nme.2021.100900.
- [21] M. Poradzinski, I. Ivanova-Stanik, G. Pelka, V. P. Ridolfini, R. Zagórski, Integrated power exhaust modelling for demo with lithium divertor, *Fusion Engineering and Design* 146 (2019) 1500–1504, sI:SOFT-30. doi:https://doi.org/10.1016/j.fusengdes.2019.02.115.
- [22] D. Andruczyk, R. Maingi, J. S. Hu, G. Z. Zuo, R. Rizkallah, M. Parsons, A. Shone, D. O'Dea, A. Kapat, M. Szott, S. Stemmley, Z. Sun, W. Xu, X. C. Meng, R. Lunsford, E. P. Gilson, A. Diallo, K. T. and, Overview of lithium injection and flowing liquid lithium results from the US-china collaboration on EAST, *Physica Scripta T171* (2020) 014067. doi:10.1088/1402-4896/ab6ce1.
- [23] E. D. Marenkov, A. S. Kukushkin, A. A. Pshenov, Modeling the vapor shielding of a liquid lithium divertor target using solps 4.3 code, *Nuclear Fusion* 61 (2021).
- [24] R. J. Goldston, R. Myers, J. Schwartz, The lithium vapor box divertor, *Phys. Scr. T167* (2016) 014017. doi:10.1088/0031-8949/T167/1/014017.
- [25] J. A. Schwartz, E. D. Emdee, R. Goldston, M. Jaworski, Physics design for a lithium vapor box divertor experiment on magnum psi, *Nuclear Materials and Energy* 18 (2019) 350–355. doi:10.1016/j.nme.2019.01.024.
- [26] V. Y. Sergeev, B. V. Kuteev, A. S. Bykov, S. V. Krylov, V. G. Skokov, V. M. Timokhin, Lithium technologies for edge plasma control, *Fusion Engineering and Design* 87 (10) (2012) 1765–1769, the 2nd International Symposium of Lithium Application for Fusion Devices. doi:10.1016/j.fusengdes.2011.10.008.
- [27] A. Bortolon, V. Rohde, R. Maingi, E. Wolfrum, R. Dux, A. Herrmann, R. Lunsford, R. M. McDermott, A. Nagy, A. Kallenbach, D. K. Mansfield, R. Nazikian, R. Neu, Real-time wall conditioning by controlled injection of boron and boron nitride powder in full tungsten wall ASDEX Upgrade, *Nuclear Materials and Energy* 19 (2019) 384 – 389. doi:10.1016/j.nme.2019.03.022.
- [28] A. Bortolon, R. Maingi, A. Nagy, J. Ren, J. Duran, A. Maan, D. Donovan, J. Boedo, D. Rudakov, A. Hyatt, T. Wilks, M. Shafer, C. Samuell, M. Fenstermacher, E. Gilson, R. Lunsford, D. Mansfield, T. Abrams, R. Nazikian, Observations of wall conditioning by means of boron powder injection in DIII-d h-mode plasmas, *Nuclear Fusion* 60 (12) (2020) 126010. doi:10.1088/1741-4326/abaf31.
- [29] E. Gilson, et al., Wall Conditioning and ELM Mitigation with Boron Nitride Powder Injection in KSTAR (2021).
- [30] Z. Sun, R. Maingi, J. Hu, W. Xu, G. Zuo, Y. Yu, C. Wu, M. Huang, X. Meng, L. Zhang, L. Wang, S. Mao, F. Ding, D. Mansfield, J. Canik, R. Lunsford, A. Bortolon, X. Gong, Real time wall conditioning with lithium powder injection in long pulse H-mode plasmas in EAST with tungsten divertor, *Nuclear Materials and Energy* 19 (2019) 124–130. doi:10.1016/j.nme.2019.02.029.
- [31] R. Maingi, J. S. Hu, Z. Sun, K. Tritz, G. Z. Zuo, W. Xu, M. Huang, X. C. Meng, J. M. Canik, A. Diallo, R. Lunsford, D. K. Mansfield, T. H. Osborne, X. Z. Gong, Y. F. Wang, Y. Y. L. and, ELM elimination with Li powder injection in EAST discharges using the tungsten upper divertor, *Nuclear Fusion* 58 (2) (2018) 024003, publisher: IOP Publishing. doi:10.1088/1741-4326/aa9e3f.
- [32] Z. Sun, A. Diallo, R. Maingi, Y. Qian, K. Tritz, Y. Wang, Y. Wang, A. Bortolon, A. Nagy, L. Zhang, Y. Duan, Y. Ye, H. Zhao, H. Wang, X. Gu, G. Zuo, W. Xu, M. Huang, C. Li, X. Meng, C. Zhou, H. Liu, Q. Zang, L. Wang, J. Qian, G. Xu, X. Gong, J. Hu, E. team, Suppression of edge localized modes with real-time boron injection using the tungsten divertor in EAST, *Nucl. Fusion* 61 (1) (2021) 014002. doi:10.1088/1741-4326/abc763.
- [33] F. Nespoli, N. Ashikawa, E. Gilson, R. Lunsford, S. Masuzaki, M. Shoji, T. Oishi, C. Suzuki, A. Nagy, A. Mollen, N. Pablant, K. Ida, M. Yoshinuma, N. Tamura, D. Gates, T. Morisaki, First impurity powder injection experiments in lhd, *Nuclear Materials and Energy* 25 (2020) 100842. doi:https://doi.org/10.1016/j.nme.2020.100842.
- [34] R. Lunsford, others, Characterization of injection and confinement improvement through impurity induced profile modifications on the wendelstein 7-x stellarator., submitted to PoP 2021.
- [35] H. Guo, H. Wang, J. Watkins, L. Casali, B. Covele, A. Moser, T. Osborne, C. Samuell, M. Shafer, P. Stangeby, D. Thomas, J. Boedo, R. Buttery, R. Groebner, D. Hill, L. Holland, A. Hyatt, A. Jaervinen, A. Kellman, L. Lao, C. Lasnier, A. Leonard, C. Murphy, J. Ren, C. Sang, A. Sontag, T. Taylor, the DIII-D Team, First experimental tests of a new small angle slot divertor on DIII-D, *Nucl. Fusion* 59 (8) (2019) 086054. doi:10.1088/1741-4326/ab26ee.
- [36] M. Shafer, B. Covele, J. Canik, L. Casali, H. Guo, A. Leonard, J. Lore, A. McLean, A. Moser, P. Stangeby, D. Taussig, H. Wang, J. Watkins, Dependence of neutral pressure on detachment in the small angle slot divertor at DIII-D, *Nuclear Materials and Energy* 19 (2019) 487–492. doi:10.1016/j.nme.2019.04.003.
- [37] L. Casali, B. Covele, H. Guo, The effect of neutrals in the new sas divertor at diii-d as modelled by solps, *Nuclear Materials and Energy* 19 (2019) 537–543. doi:https://doi.org/10.1016/j.nme.2019.04.003.

- [//doi.org/10.1016/j.nme.2019.03.021](https://doi.org/10.1016/j.nme.2019.03.021).
- [38] O. Février, H. Reimerdes, C. Theiler, D. Brida, C. Colandrea, H. De Oliveira, B. Duval, D. Galassi, S. Gorno, S. Henderson, M. Komm, B. Labit, B. Linehan, L. Martinelli, A. Perek, H. Raj, U. Sheikh, C. Tsui, M. Wensing, Divertor closure effects on the tcv boundary plasma, *Nuclear Materials and Energy* 27 (2021) 100977. doi:10.1016/j.nme.2021.100977.
 - [39] T. Morisaki, S. Masuzaki, M. Kobayashi, M. Shoji, J. Miyazawa, R. Sakamoto, G. Motojima, M. Goto, H. Funaba, H. Tanaka, K. Tanaka, I. Yamada, S. Ohdachi, H. Yamada, A. K. and, Initial experiments towards edge plasma control with a closed helical divertor in LHD, *Nuclear Fusion* 53 (6) (2013) 063014. doi:10.1088/0029-5515/53/6/063014.
 - [40] T. Abrams, R. Ding, H. Guo, D. Thomas, C. Chrobak, D. Rudakov, A. McLean, E. Unterberg, A. Briesemeister, P. Stangeby, J. Elder, W. Wampler, J. Watkins, The inter-ELM tungsten erosion profile in DIII-d h-mode discharges and benchmarking with ero+oedge modeling, *Nuclear Fusion* 57 (5) (2017) 056034. doi:10.1088/1741-4326/aa66b2.
 - [41] L. Casali, D. Eldon, A. G. McLean, T. H. Osborne, A. W. Leonard, B. A. Grierson, J. Ren, Impurity leakage and radiative cooling in the first nitrogen and neon seeding study in the slot divertor at diii-d, *Nuclear Fusion* (2021).
 - [42] H. P. Summers, N. R. Badnell, M. G. O'Mullane, A. D. Whiteford, R. Bingham, B. J. Kellett, J. Lang, K. H. Behringer, U. Fantz, K.-D. Zastrow, S. D. Loch, M. S. Pindzola, D. C. Griffin, C. P. Ballance, Atomic data for modelling fusion and astrophysical plasmas, *Plasma Physics and Controlled Fusion* 44 (12B) (2002) B323.
 - [43] A. Nagy, A. Bortolon, D. M. Mauzey, E. Wolfe, E. P. Gilson, R. Lunsford, R. Maingi, D. K. Mansfield, R. Nazikian, A. L. Roquemore, A multi-species powder dropper for magnetic fusion applications, *Review of Scientific Instruments* 89 (10) (2018) 10K121, eprint: <https://doi.org/10.1063/1.5039345>. doi:10.1063/1.5039345.
 - [44] M. E. Fenstermacher, W. H. Meyer, R. D. Wood, D. G. Nilson, R. Ellis, N. H. Brooks, A tangentially viewing visible TV system for the DIII-D divertor, *Review of Scientific Instruments* 68 (1) (1997) 974–977. doi:10.1063/1.1147729.
 - [45] W. W. Heidbrink, P. L. Taylor, J. A. Phillips, Measurements of the neutron source strength at diii-d, *Review of Scientific Instruments* 68 (1) (1997) 536–539. [arXiv:https://doi.org/10.1063/1.1147646](https://doi.org/10.1063/1.1147646), doi:10.1063/1.1147646. URL <https://doi.org/10.1063/1.1147646>
 - [46] T. Petrie, B. Grierson, T. Osborne, C. Petty, F. Turco, S. Allen, M. Fenstermacher, J. Ferron, H. Guo, E. Hinson, R. L. Haye, C. Lasnier, A. Leonard, A. McLean, B. Victor, H. Wang, J. Watkins, High performance double-null plasmas under radiating divertor and mantle scenarios on DIII-d, *Nuclear Fusion* 59 (8) (2019) 086053. doi:10.1088/1741-4326/ab2936.
 - [47] W. Xu, J. S. Hu, Z. Sun, R. Maingi, L. Zhang, Y. W. Yu, C. L. Li, G. Z. Zuo, Y. Z. Qian, M. Huang, X. C. Meng, W. Gao, Y. M. Duan, Y. J. Chen, K. Wang, X. D. Lin, X. Gao, Effect of lithium coating on long pulse high performance plasma discharges in EAST, *Plasma Physics and Controlled Fusion* 62 (8) (2020) 085012. doi:10.1088/1361-6587/ab9b3a.
 - [48] R. Raman, W.-S. Lay, T. Jarboe, J. Menard, M. Ono, Electromagnetic particle injector for fast time response disruption mitigation in tokamaks, *Nuclear Fusion* 59 (1) (2018) 016021. doi:10.1088/1741-4326/aaf192.